



HAL
open science

Dynamic characteristics analysis of a rotor–stator system under different rubbing forms

Hui Ma, Qianbin Zhao, Xueyan Zhao, Qingkai Han, Bangchun Wen

► **To cite this version:**

Hui Ma, Qianbin Zhao, Xueyan Zhao, Qingkai Han, Bangchun Wen. Dynamic characteristics analysis of a rotor–stator system under different rubbing forms. *Applied Mathematical Modelling*, 2015, 39 (8), pp.2392 - 2408. 10.1016/j.apm.2014.11.009 . hal-01396070

HAL Id: hal-01396070

<https://hal.science/hal-01396070>

Submitted on 13 Nov 2016

HAL is a multi-disciplinary open access archive for the deposit and dissemination of scientific research documents, whether they are published or not. The documents may come from teaching and research institutions in France or abroad, or from public or private research centers.

L'archive ouverte pluridisciplinaire **HAL**, est destinée au dépôt et à la diffusion de documents scientifiques de niveau recherche, publiés ou non, émanant des établissements d'enseignement et de recherche français ou étrangers, des laboratoires publics ou privés.



Distributed under a Creative Commons Attribution 4.0 International License

Dynamic characteristics analysis of a rotor–stator system under different rubbing forms

Hui Ma ^{a,*}, Qianbin Zhao ^a, Xueyan Zhao ^b, Qingkai Han ^c, Bangchun Wen ^a

^a School of Mechanical Engineering and Automation, Northeastern University, Shenyang, Liaoning 110819, PR China

^b Department of Automatic Control and Systems Engineering, University of Sheffield, Mappin Street, Sheffield, South Yorkshire S1 3JD, UK

^c School of Mechanical Engineering, Dalian University of Technology, Dalian, Liaoning 116023, PR China

Dynamic characteristics of a rotor rubbing with circular stator and four pin shape stators are studied based on contact dynamics theory. Based on finite element (FE) method, the rotor system attached with two disks and pin shape stators are simulated by Timoshenko beam. The circular stator is simulated by a lumped mass model, and the rotor and stator are connected by one or more point point contact elements to establish the dynamic model of the rotor stator coupling system. Assuming that the rubbing is caused by the sudden impact excitation and sudden unbalance excitation under two loading conditions (condition 1: in phase unbalances of two disks at the first critical speed, condition 2: out of phase unbalances of two disks at the second critical speed), the system dynamic characteristics are analyzed by the time domain waveform, rotor orbit, normal contact/rubbing force and stator acceleration. The results show that the rubbing caused by the sudden impact under the loading condition 2 will always exist and the rubbing will excite quasi periodic motion of the rotor system; combination frequency components about the rotating frequency ($1\times$) and the first lateral natural frequency of the rotor stator coupling system (f_{n1}) can be viewed as the most distinguishable characteristic. Full annular rubbing may appear due to the sudden unbalance excitation under the loading condition 1, the four point rubbing can restrain the subsynchronous vibration and mainly excites odd multiple frequency components, such as $3\times$ and $5\times$.

Keywords: Rubbing, Finite element, Rotor system, Dynamic characteristic, Combination frequency components

1. Introduction

Rotor stator clearance is one of the important parameters influencing the properties of the rotating machinery. To improve the performance and efficiency of the rotating machinery, a key design for such improvements is widely adopted by minimizing the operational clearances between the rotor and stator. However, the probability of the rotor stator rubbing increases with the decreasing clearance, which has long been identified as a significant contributor to excessive maintenance and in general to engine failure. The rubbing may result in complicated vibration of the overall unit, and may also reduce system performance and the lives of the rotor and the stator.

In rotor systems, the rubbing forms mainly include three forms: point rubbing, partial rubbing and full annular rubbing. Point rubbing often occurs when the stator stiffness is greater than the rotor stiffness. Under this condition, the rubbing force

can change the motion direction of the rotor. Aiming at the point rubbing, lots of studies [1–6] have been carried out. Han et al. [1] analyzed periodic motions of a rotor system with two disks where the rub impacts occur at fixed limiter for a test rig with dual disks. By a point–point contact model, Ma et al. [2] investigated fault characteristics of a single span rotor system with two disks when the rubbing between a disk and an elastic rod occurs. In order to reduce the rub related severity in friction, Lahri et al. [3,4] developed a new unconventional backup bearing, which utilizes four pin connections to force the rotor to the center and mitigate the lateral motion. In this way, the full annular rubbing can be changed into four point rubbing. Based on finite element (FE) theory with unilateral contact and friction conditions, Behzad et al. [5] developed an algorithm to investigate of the rotor to stator rubbing vibration and carried out a case study of the point rubbing between the rotor and an elastic rod by using this algorithm. Isaksson and Frid [6] studied the dynamical behavior of a rotor rubbing with a non annular stator and analyzed the influences of different stop configurations on the system vibration responses. Zapomel et al. [7] simulated the impacts between the rotor and its housing based on the application of Newton's theory and on the direct calculation of the contact force and investigated the behavior of rotor systems when the impact occurs.

Partial rubbing is the most common among the three rubbing forms, which denotes that the rotor partially rubs a small portion of the stator periphery. Partial rubbing between the rotor and stator are also extensively investigated in the literatures [8–17]. Beatty [8] analyzed the rotor response due to the radial rubbing, which is described as a function of the rotor contact circumference based on a combination of analytical and experimental results. Based on a numerical model and an experimental set up, Torkhani et al. [9] investigated the partial rub of a rotor when the rotor contacts the non rotating obstacle under partial light, medium and severe rubs conditions. Abuzaid et al. [10] analyzed the vibration responses of a partial rotor to stator rubbing both experimentally and analytically. Their results indicate that vibrations induced by light rubbing are characterized by the integral multiple rotational frequency and severe rubbing by $1/3$ and $2/3$ multiple rotational frequency. Choi [11] investigated the partial rotor rub experimentally and analytically to understand the rubbing phenomenon. To reproduce what happens in real systems when the shaft line interferes with labyrinth seals, Pennacchi et al. [12] presented an experimental study and a mathematical model and analyzed the effects of rotor to stator rub on seals. Zhang et al. [13] presented a rub impact micro rotor model with scaling nonlinear rub impact force and investigated the nonlinear dynamic characteristics of micro electro mechanical systems (MEMS). Popprath and Ecker [14] presented a Jeffcott rotor model with intermittent contact with a stator interacting with the rotor model via non linear contact forces. The sub model of the stator was modeled as an additional vibratory system. In order to investigate the nonlinear characteristics of a rotor intermittently contacting with a stator, Patel et al. [15] established a mathematic model consisting of rotor and stator vibratory systems and analyzed the nonlinear lateral torsional vibration characteristics of a rotor contacting with a viscoelastically suspended stator. Chu and Lu [16] designed a special structure of stator to simulate rub, and studied the nonlinear vibration of a rub impact rotor system, and observed a variety of periodic and chaotic vibrations. Bachschmid et al. [17] designed a rotor test rig, which is similar to full size rotating machines, and presented a simulation experiment involving the rubbing of a shaft and a partial seal ring. The results show that higher harmonic components in proximity probe signals in bearings can be used to identify even light rubs, and the torsional vibrations seem to be rather unaffected by the partial rub.

Full annular rubbing shows that the rotor is in continuous contact with the stator, which usually occurs under large unbalance, such as the sudden unbalance due to broken blades. In order to explain the onset and disappearance of the backward whirling motion of full annular rotor rub, Choi [18] performed an experiment and the numerical analysis for the experiment. Jiang and Ulbrich [19] presented a modified Jeffcott rotor with a given rotor/stator clearance and cross coupling influences and carried out an analytical study on the stability of the full annular rub solutions. Childs and Kumar [20] developed analytic dry friction whip and whirl solutions for a rigid rotor/rigid stator model with contact at two rubbing locations. Yu [21] discussed the reverse full annular rub based on a two degree of freedom rotor/seal model where a rubbing location can be simulated away from the lumped rotor mass and compared the results of the analytical model with the experimental results. Considering the transient response of an overcritical high speed rotor, Grapis et al. [22] analyzed a series of rotor–stator collisions succeeded by full annular rub initiated by a rapid increase of unbalance. Lu and Chu [23] analyzed the dynamics characteristics, whirl and torsional vibrations of a vertical Jeffcott rotor under no rub, full annular rub and partial rub conditions. Dai et al. [24] studied the forced nonlinear vibration of a rotor rubbing with motion limiting stops by means of numerical method. Their results show that the stop can limit the vibration amplitude of the rotor which whirls violently at the low frequency under the stable partial rubbing condition. With the increase of the amplitudes of the excitation, the partial rubbing will expand to full rubbing in which the rotor keeps contact with the stop.

In real rotating machines, rub induced thermal impact plays a primary role. Some researchers carried out theoretical and experimental investigations considering the effects related to shaft heating due to rubbing. Kellenberger [25] investigated the synchronous rotor instability due to generator hydrogen seal rings under various combinations of support conditions. His results show that the mechanism for the production of a hot spot on the shaft is friction in a rub and the Morton effect is concerned with a thermohydrodynamic source of shaft heating. Childs [26] extended the Kellenberger model to include the effects of a radial clearance at the rub location. Goldman and Muszynska [27] discussed the thermal effects of the rotor to stator rub and analyzed their influence on the rotor vibration response. Sawicki et al. [28] presented an analytical study of the dynamics and stability of rotors subjected to rubbing, taking account of associated thermal effects. Considering the rub induced force impact and heat impact together, Tian and Yang [29] developed a coupled set of equations to analyze the dynamic response of a rubbing rotor and analyzed the temperature distribution, contact force, thermal bending and vibration characteristics by using the new model. Bachschmid et al. [30] developed a model to analyze “spiral vibrations”

or “thermally induced vibrations” of full size rotors caused by rub and validated the capability of the proposed method to reproduce the behavior of real machines by an experimental case of rub of a 50 MW generator.

The mechanical model of the rotor stator rubbing mostly adopts the piecewise smooth model and the classical coulomb friction model [1,3,4,6,12,13,15,22,24]. In recent years, the rotor stator rubbing simulated by the contact theory has become widely researched [2,5,9,31–35]. Based on the above analysis, we found that some researchers adopted non annular stator [6] (passive mechanical deflection limiting device) or four pin connections [2,3] to prevent vital rotor or stator parts from coming into contact or make possible full annular rubbing transmit local fixed point rubbing to protect the bearing. At present, there are few investigations about the suppression or control of rotor vibration by changing stator structures, which may change the rubbing forms. Based on the present literatures, this paper will focus on the effects of different rubbing forms: fixed point rubbing and partial/full annular rubbing on dynamic characteristics of the rotor and stator based on the contact theory. It is expected that the simulation method and results can provide some thoughts to simulate the rotor vibration caused by rubbing.

This paper consists of five sections. After this introduction, rotor stator rubbing models and finite element model of a rubbing rotor stator system are developed in Section 2. In Section 3, fixed point rubbing model validation is carried out by comparing the experimental results in reference with simulation results in this paper. In Section 4, annular rubbing and four point rubbing excited by the sudden impact excitation and sudden unbalance excitation are simulated under two loading conditions. Finally, conclusions are drawn in Section 5.

2. Finite element modeling

A flexible rotor bearing system, attached with two disks, is shown in Fig. 1. In order to study the rotor bearing system efficiently, the FE model of the rotor bearing system is simplified according to the following assumptions:

- The shaft is divided into 24 Timoshenko beam elements and 25 nodes; every node has four degrees of freedom as is shown in Fig. 2. In the figure, z_A , y_A and θ_{zA} , θ_{yA} denote displacements in translation directions and angular displacements in rotation directions, subscripts A and B denote nodes A and B in shaft, respectively.
- Two rigid disks are simulated by lumped mass elements and superimposed upon the corresponding nodes, which are specified by the mass m_d , the diametral and polar mass moments of inertia (I_d and I_p), meanwhile the gyroscopic effects of the disks are also considered. In Fig. 2, subscripts C denotes node C , which is used to simulate the rigid disk. The detailed information about the lumped mass element can be found in Appendix A. In this paper, two disks are identical with $m_d = 0.5674$ kg, $I_d = 2.5 \times 10^{-4}$ kg m² and $I_p = 4.7 \times 10^{-4}$ kg m².
- For the sliding bearing, the oil film commonly provides nonlinear elastic and damping forces, but in most cases, the oil film force can be simplified as linear elastic and damping forces when the journal is apart from the balance position slightly. In such a case, the bearing can be modeled as a stiffness damping form; stiffness, cross stiffness, damping and

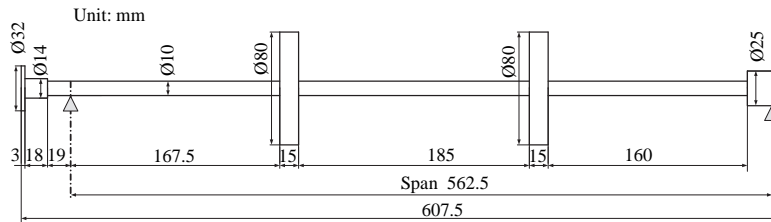


Fig. 1. Geometric dimensions of a flexible rotor system.

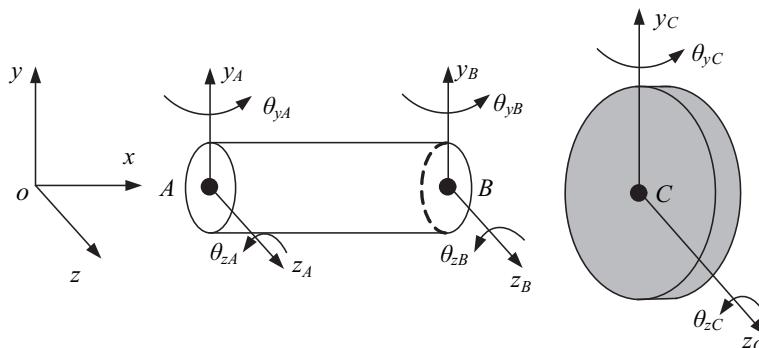


Fig. 2. FE model of a shaft element and a rigid disk.

cross damping coefficients in horizontal (z coordinate) and vertical (y coordinate) directions should be considered. In this paper, the cross terms are neglected, and the left and right bearings are simulated ideally by identical linear stiffness and damping coefficients in y and z directions.

Neglecting axial and torsional displacements, the general displacement vector of a beam element for the shaft \mathbf{u}_r is given as

$$\mathbf{u}_r = [y_A \ z_A \ \theta_{y_A} \ \theta_{z_A} \ y_B \ z_B \ \theta_{y_B} \ \theta_{z_B}]^T. \quad (1)$$

The general displacement vector of a rigid disk \mathbf{u}_d is given as

$$\mathbf{u}_d = [y_C \ z_C \ \theta_{y_C} \ \theta_{z_C}]^T. \quad (2)$$

2.1. Rotor stator rubbing models

In order to simulate the rotor stator rubbing efficiently, the rubbing model is simplified according to the following assumptions:

- (a) For partial/full annular rubbing, the rotor and stator are simplified as two rigid points and the support stiffness of the stator is simulated by two spring damping elements in z and y directions (see Fig. 3(a)). k_{sz} , c_{sz} , k_{sy} and c_{sy} denote the stiffness and damping coefficients in z and y directions, respectively.
In Fig. 3, o is the center of the stationary rotor, o_r the geometric center of the rotor and ω the rotating speed. The rubbing is simulated by a point-point contact element where the master body is set as the rotor and the slave one is the stator. It is assumed that the cross section of the disk remains in the yo_z plane. Point c in the disk and point d in the stator are selected as a contact pair shown in Fig. 3, so the gap function g is equal to the distance \overline{cd} .
- (b) For the four-point rubbing, four pin shape stators are simulated by four Timoshenko beams where only axial degree of freedom (DOF) is considered. The support stiffness of the stator is also simulated by the spring damping element. The stiffness and damping of the stator in z and y directions are all the same, and denoted by k_{sz} , c_{sz} , k_{sy} and c_{sy} , respectively. Four point-point contact elements are used to simulate rubbing (see Fig. 3(b)). In Fig. 3(b), the numbers denote the stator positions. For example, "1" denotes that the stator locates in positive z direction.
- (c) Thermal effects and friction torque during the rubbing between the rotor and the stator are not considered, and only transverse motion of the rotor is considered.

Generally, normal contact force F_N can be expressed as the product of a non-negative scalar F_N and the unit outward vector \mathbf{n} . Likewise, tangential contact force $\mathbf{F}_T = F_T \mathbf{t}$ where F_T is a non-negative scalar and \mathbf{t} the unit tangent vector. Based on contact dynamic theory [36–38], two contact points c and d must satisfy the following Kuhn-Tucker impenetrability conditions:

$$\begin{cases} F_N \geq 0, \\ g \leq 0, \\ F_N \cdot g = 0. \end{cases} \quad (3)$$

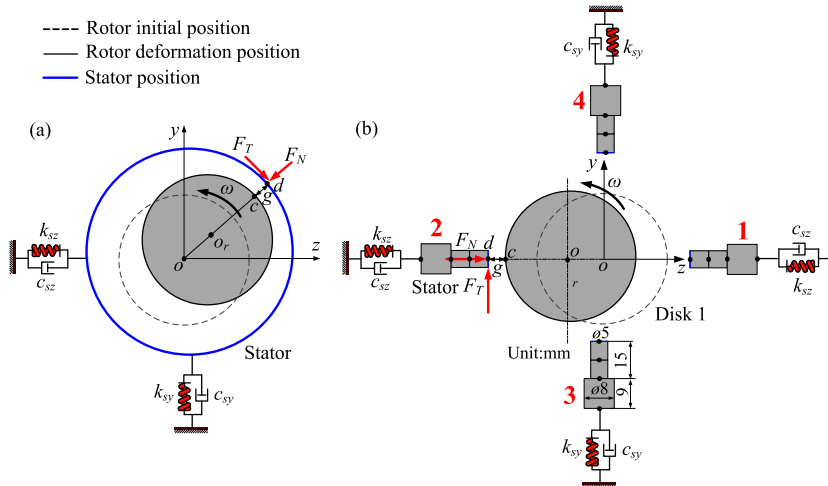


Fig. 3. Rubbing model schematic: (a) partial/full annular rubbing, (b) fixed-point rubbing.

Eq. (3) implies the vanishing of F_N in the case of separation or the vanishing of g in the case of contact.

Friction is often an essential consideration for a contact problem. Although various friction schemes have been proposed, the Coulomb friction law is still one of the most widely accepted models to describe the friction phenomenon. The Kuhn Tucker conditions for Coulomb friction are as follows:

$$\phi \quad \|\mathbf{F}_T\| \quad \mu_f F_N \leq 0, \quad (4)$$

$$\dot{\mathbf{g}}_T \quad \xi \frac{\partial}{\partial \mathbf{F}_T} \phi, \quad (5)$$

$$\begin{cases} \xi \geq 0, \\ \xi \phi = 0, \end{cases} \quad (6)$$

where $\|\cdot\|$ denotes L2 norm, μ_f is the friction coefficient and \mathbf{g}_T is the tangential gap. According to Eqs. (5) and (6), it is clear that the perfect stick contact occurs when $\phi < 0$ and slip contact occurs when $\phi = 0$.

The augmented Lagrangian method is adopted to deal with contact constraint conditions. The augmented Lagrangian statement of the friction law is expressed as follows:

$$\begin{cases} F_N = \langle \lambda_N + \varepsilon_N \mathbf{g} \rangle, \\ \phi \quad \|\mathbf{F}_T\| \quad \mu_f F_N \leq 0, \\ \dot{\mathbf{g}}_T \quad \xi \frac{\partial}{\partial \mathbf{F}_T} \phi \quad \frac{1}{\varepsilon_T} (\dot{\mathbf{F}}_T \quad \dot{\lambda}_T), \\ \xi \geq 0, \\ \xi \phi = 0, \end{cases} \quad (7)$$

where $\varepsilon_N > 0$ is the penalty parameter in the normal direction (normal contact stiffness) and λ_N is the Lagrange multiplier. The tangential traction \mathbf{F}_T contains the penalty part and the Lagrange multiplier part wherein λ_T denotes the tangential Lagrange multiplier of \mathbf{F}_T , and ε_T is the tangent penalty parameter. Assuming that the system response at $t = T_n$ is known, the complete augmentation equations for the contact tractions are listed as follows:

$$\begin{cases} F_{N_{n+1}} = \langle \lambda_{N_{n+1}} + \varepsilon_N \mathbf{g}_{n+1} \rangle \\ \mathbf{F}_{T_{n+1}} = \mathbf{F}_{T_n} + \Delta \lambda_T + \varepsilon_T (\Delta \mathbf{g}_T \quad \Delta \xi \mathbf{F}_{T_{n+1}}^{\text{trial}} / \|\mathbf{F}_{T_{n+1}}^{\text{trial}}\|) \end{cases} \quad (8)$$

where

$$\begin{cases} \Delta \lambda_T = \lambda_{T_{n+1}} - \lambda_{T_n}, \\ \Delta \mathbf{g}_T = \mathbf{g}_{T_{n+1}} - \mathbf{g}_{T_n}, \\ \mathbf{F}_{T_{n+1}}^{\text{trial}} = \mathbf{F}_{T_n} + \Delta \lambda_T + \varepsilon_T \Delta \mathbf{g}_{T_{n+1}}, \\ \Delta \xi = \begin{cases} 0, & \phi_{n+1}^{\text{trial}} \leq 0, \\ \frac{\phi_{n+1}^{\text{trial}}}{\varepsilon_T}, & \phi_{n+1}^{\text{trial}} > 0, \end{cases} \end{cases} \quad (9)$$

2.2. Finite element model of a rotor-stator system with rubbing

Considering the effects of rubbing and the external forces on the system vibration, the equation of motion of the rotor-stator system can be written as follows:

$$\begin{bmatrix} \mathbf{M}_r & \mathbf{0} & \mathbf{0} \\ \mathbf{0} & \mathbf{0} & \mathbf{0} \\ \mathbf{0} & \mathbf{0} & \mathbf{M}_s \end{bmatrix} \begin{bmatrix} \ddot{\mathbf{u}}_r \\ \mathbf{0} \\ \ddot{\mathbf{u}}_s \end{bmatrix} + \begin{bmatrix} \omega \mathbf{G} + \mathbf{C}_r & \mathbf{0} & \mathbf{0} \\ \mathbf{0} & \mathbf{0} & \mathbf{0} \\ \mathbf{0} & \mathbf{0} & \mathbf{C}_s \end{bmatrix} \begin{bmatrix} \dot{\mathbf{u}}_r \\ \mathbf{0} \\ \dot{\mathbf{u}}_s \end{bmatrix} + \begin{bmatrix} \mathbf{K}_r + \varepsilon_N \mathbf{B}^T \mathbf{B} & \mathbf{B}^T & \mathbf{0} \\ \mathbf{B}^T & \mathbf{0} & \mathbf{B}^T \\ \mathbf{0} & \mathbf{B}^T & \mathbf{K}_s + \varepsilon_N \mathbf{B}^T \mathbf{B} \end{bmatrix} \begin{bmatrix} \mathbf{u}_r \\ \lambda \\ \mathbf{u}_s \end{bmatrix} = \begin{bmatrix} \mathbf{F}_u & \varepsilon_N \mathbf{B}^T \mathbf{g}_0 \\ \mathbf{g}_0 \\ \varepsilon_N \mathbf{B}^T \mathbf{g}_0 \end{bmatrix}, \quad (10)$$

where \mathbf{M} , $\omega \mathbf{G}$, \mathbf{C} , \mathbf{K} and \mathbf{u} respectively denote the mass matrix, the gyroscopic matrix, the damping matrix (for the rotor, the bearing damping and viscous damping of the rotor are included, for the stator, the viscous damping and support damping of the stator are included) and the stiffness matrix (for the rotor, the rotor stiffness and the bearing stiffness are included, for the stator, the support stiffness of the stator is included) and the displacement vector of the global system respectively. Here, subscripts "r" and "s" stand for the rotor and stator. λ is a vector about the Lagrange multiplier, \mathbf{B} is the contact constraint matrix in the normal and tangential directions, \mathbf{g}_0 is the initial normal gap vector, and \mathbf{F}_u is the external load vector. In this paper, Rayleigh damping form is applied to determine the viscous part (\mathbf{C}_v) of the total damping matrix (\mathbf{C}_r and \mathbf{C}_s) and it can be obtained by the following formula [39]:

$$\mathbf{C}_v = \alpha \mathbf{M} + \beta \mathbf{K}, \quad (11)$$

where

$$\begin{cases} \alpha & \frac{\pi\omega_{n1}\omega_{n2}(\xi_1\omega_{n2} - \xi_2\omega_{n1})}{15(\omega_{n2}^2 - \omega_{n1}^2)}, \\ \beta & \frac{60(\xi_2\omega_{n2} - \xi_1\omega_{n1})}{\pi(\omega_{n2}^2 - \omega_{n1}^2)}, \end{cases} \quad (12)$$

herein ω_{n1} and ω_{n2} respectively stand for the first and second critical speeds (rev/min) of the rotor system, ξ_1 and ξ_2 are corresponding modal damping ratios, respectively. The global matrixes are assembled by the corresponding element matrixes. Element matrixes of Timoshenko beam can be found in Ref. [40], the stiffness and damping matrixes of the bearing in Ref. [2], element matrixes of rotating disks (rigid disk) and stators are shown in Appendix A.

The FE model of a rubbing rotor system is shown in Fig. 4. In the figure, the number denotes the node number, node 10 the position of disk 1 and the rub impact occurs at node 10. Nonlinear differential equations considering the rotor-stator rubbing Eq. (10), is solved by using Newmark β method combined with Newton-Raphson iteration.

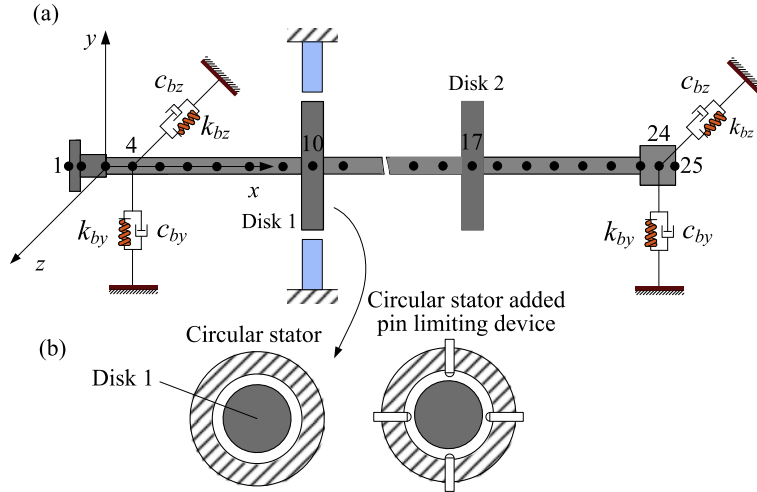


Fig. 4. FE model of a rotor system with rubbing: (a) schematic of rotor (b) rubbing schematic.

Table 1
Model parameters of the rotor system.

Material parameters of rotor	Elastic modulus E (GPa)	Poisson's ratio ν	Density ρ (kg/m ³)	The first and second modal damping ratios ($\xi_1 = \xi_2$)
	207	0.3	7850	0.04
Material parameters of the stator	Elastic modulus E (GPa)	Poisson's ratio ν	Density ρ (kg/m ³)	-
	90	0.3	8800	
Bearing parameters	Horizontal stiffness k_{bz} (MN/m)	Vertical stiffness k_{by} (MN/m)	Horizontal damping c_{bz} (kN s/m)	Vertical damping c_{by} (kN s/m)
	10	20	2	2
Pin shape stator parameters	Normal stiffness (MN/m)	Normal damping (kN s/m)	Geometric dimensions of the pin shape stator	-
	6	0	See Fig. 3	
Circular shape stator parameters	Horizontal stiffness k_{sz} (MN/m)	Vertical stiffness k_{sy} (MN/m)	Horizontal and vertical damping (kN s/m)	Stator mass m_s (kg)
	6	9	0	0.7
Loading condition 1	Eccentricity of unbalance mass of disk 1 mr (g m)	Eccentric phase angle of unbalance mass at disk 1 ($^\circ$)	Eccentricity of unbalance mass of disk 2 mr (kg m)	Eccentric phase angle of unbalance mass at disk 2 ($^\circ$)
	0.156	0	0.156	0
Loading condition 2	Eccentricity of unbalance mass of disk 1 mr (g m)	Eccentric phase angle of unbalance mass at disk 1 ($^\circ$)	Eccentricity of unbalance mass of disk 2 mr (kg m)	Eccentric phase angle of unbalance mass at disk 2 ($^\circ$)
	0.156	0	0.156	180
Parameters about rubbing	Normal contact stiffness e_N (MN/m)	Friction coefficient μ_f	-	-
	80	0.3		

Note: - Denotes no value.

The geometric dimensions of the rotor system can be found in Fig. 1, other model parameters of the rotor system with rubbing are listed in Table 1. The first and second critical speeds (ω_{n1} and ω_{n2}) of the rotor system without faults are 1680 rev/min and 6450 rev/min based on the parameters in Table 1.

3. Model validation

In order to verify the validity of the fixed point rubbing model presented in this paper, we will compare our simulation results based on our model parameters with the experimental results in Ref. [41]. Assuming that the rubbing only occurs at negative direction of z axis (see Fig. 3(a)) and dimensionless initial clearance δ is the ratio of the clearance of the rotor and stator and the amplitude in z direction, here, $\delta = 0.95$ under different dimensionless rotating speeds ($\gamma = \omega/\omega_{n1}$). Spectrum cascade under these parameters is shown in Fig. 5(a). The figure shows the subharmonic vibration under the light fixed point rubbing condition. With the increase of rotating speed from $\gamma = 0.5$ to $\gamma = 10$ in an increment of 0.5, a change of the subharmonic order from the order $1/2$, to the lower range $1/3$, $1/4$, $1/5$ and $1/6$. Only $1 \times$ synchronous vibration appears at $\gamma \in [0.5, 2]$, $1 \times/2$ subsynchronous vibration (period two motion P2) at $\gamma \in [2.5, 4]$, $1 \times/3$ subsynchronous vibration (P3) at $\gamma \in [4.5, 5.5]$, $1 \times/4$ subsynchronous vibration (P4) at $\gamma \in [6, 7.5]$, $1 \times/5$ subsynchronous vibration (P5) at $\gamma \in [8, 9.5]$ and $1 \times/6$ subsynchronous vibration (P6) at $\gamma = 10$. Compared with the experimental results in Ref. [41] (see Fig. 5(b)), it is clear that the change law of the simulation results is the same as that of the experimental results. The similar bifurcation laws are also described in Ref. [5].

System vibration responses under different γ are shown in Fig. 6. From the left to the right, the figure displays the rotor orbit, normal contact/rubbing force, stator acceleration, respectively. Rotor orbits corresponding to period n motions shows n ($n = 2, 3, 4, 5, 6$) loops, which indicates that the rotor contacts the stator once per n rotor revolutions. The rotor rebounds and the impacts on the stator are aggravated with the increasing rotating speed, which can be observed by rotor orbits, normal contact forces and stator accelerations. The appearance of subharmonic vibration components with frequencies being exact fractions of the rotating speed, is referred to as a result of transient free lateral vibrations of the rotor, which always correspond to the rotor damped natural frequencies [41].

4. Annular rubbing and four fixed-point rubbing simulation

Based on the API Standard 617 [42], two different unbalance loading conditions are determined according to the modal shape of the system, as is shown in Fig. 7. The detailed parameters for two conditions can be found in Table 1. Unbalance responses of disk 1 (node 10) without rubbing in z direction under two loading conditions are shown in Fig. 8. From the figure, it can be seen that the first order resonant response is predominant under loading condition 1, however the second order resonant response is predominant under loading condition 2. It means that the first loading condition excites the first mode easily and the second loading condition excites the second mode easily. The first two order critical speeds are identified as 27 Hz and 105.5 Hz according to peak points, respectively. In this study, two other specific excitations: sudden impact and

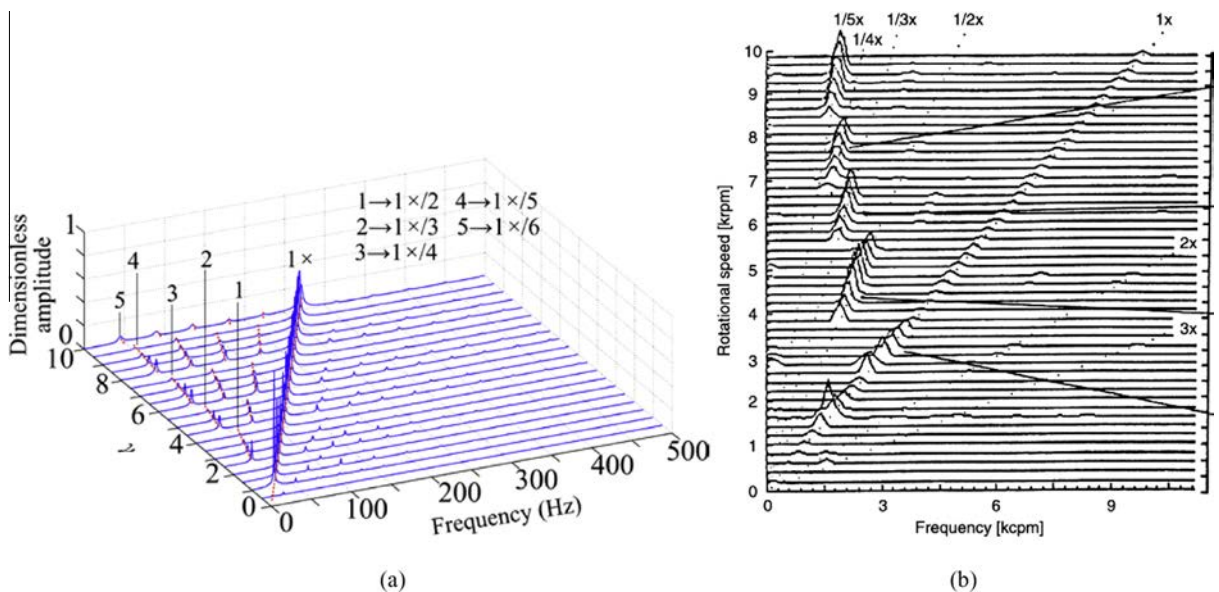


Fig. 5. Fault feature comparison under fixed-point rubbing condition: (a) simulation result for fixed-point rubbing in this paper, (b) experimental result for partial rubbing in Ref. [41].

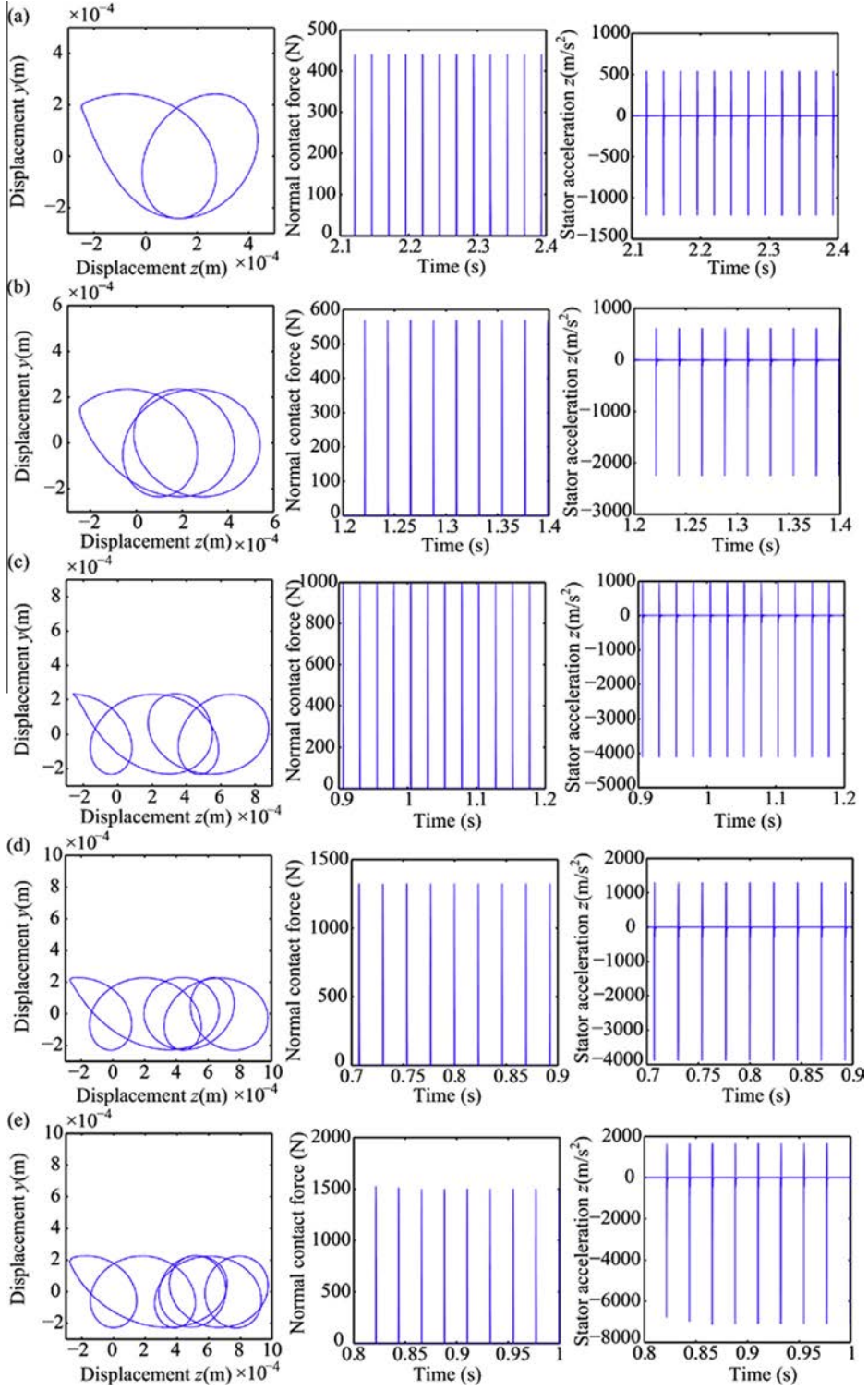


Fig. 6. Vibration responses of rotor and stator under different γ : (a) $\gamma = 3$, (b) $\gamma = 5$, (c) $\gamma = 6$, (d) $\gamma = 8$, (e) $\gamma = 10$.

sudden unbalance excitations are added to cause rubbing under two loading conditions. Two types of sudden excitations under loading condition 2 are shown in Fig. 9. At 61.5 rotating periods, sudden half sine pulse excitation (see Fig. 9(a)) is applied along 45 degree angle direction between the negative y and negative z axis whose amplitude is 80 N and its frequency is 250 Hz. At 60 rotating periods, sudden unbalance excitation (see Fig. 9(b)) is applied, whose frequency is still

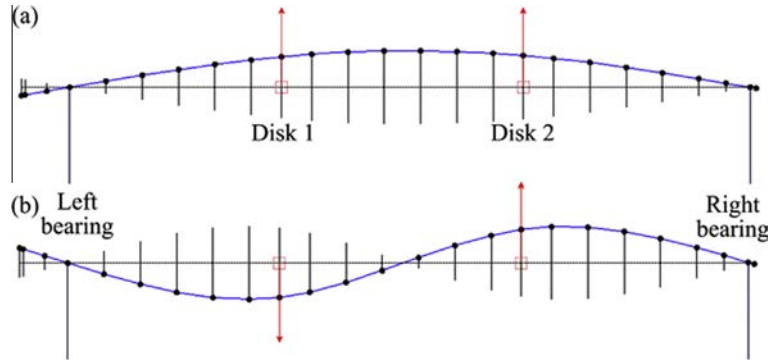


Fig. 7. Two loading conditions: (a) condition 1, (b) condition 2.

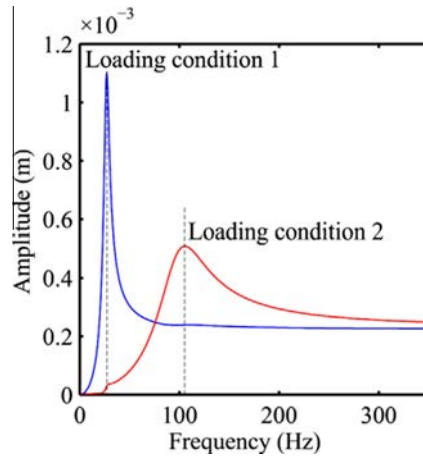


Fig. 8. Unbalance responses under two loading conditions.

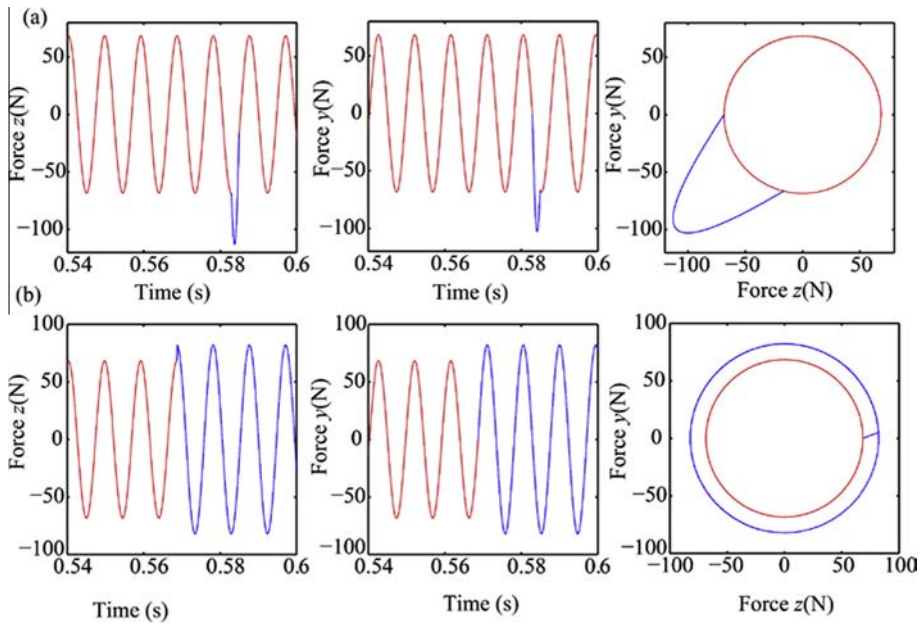


Fig. 9. Sudden excitation loads under loading condition 2: (a) sudden impact excitation, (b) sudden unbalance excitation.

Table 2
Simulation cases.

Rubbing forms	Sudden excitations	Loading conditions	Cases	Corresponding figures
Annular rubbing	Impact	1 (27 Hz)	1	Fig. 10
	Impact	2 (105.5 Hz)	2	Fig. 11
	Unbalance	1 (27 Hz)	3	Fig. 12
	Unbalance	2 (105.5 Hz)	4	Fig. 13
Four-point rubbing	Impact	1 (27 Hz)	5	Fig. 14
	Impact	2 (105.5 Hz)	6	Fig. 15
	Unbalance	1 (27 Hz)	7	Fig. 16
	Unbalance	2 (105.5 Hz)	8	Fig. 17

the rotating frequency and amplitude is 1.2 times its initial value. Eight cases can be determined in Table 2 considering different rubbing forms, sudden excitations and loading conditions.

4.1. Annular rubbing simulation

4.1.1. Sudden impact excitation

It is assumed that the ratio of the clearance of rotor and stator and the amplitude in z direction δ is 1.05 under annular rubbing condition. System vibration responses (node 10) with annular rubbing caused by the sudden impact excitation under loading condition 1 are shown in Fig. 10. The above three figures from the left to the right, are the time domain waveform, amplitude spectrum and rotor orbit, respectively. The below two figures from the left to the right are the normal contact force and stator acceleration (Figs. 11–13 with the same layouts as Fig. 10). Fig. 10 shows that the rubbing appears under the action of sudden impact excitation, lasts for a short time about 4.3 ms and disappears by undergoing 10 times collisions. The collision degree can also be identified by the stator vibration, which is closely related to the normal contact force.

System vibration responses under loading condition 2 (case 2) are shown in Fig. 11. The figure indicates that the rubbing always exists even though the sudden impact force disappears. The collision degree is considerably larger than that in case 1 by comparing waveform, normal contact force and stator acceleration. Experiencing multiple continuous collisions, the rotor will be rebounded and system motion will translate to transient free lateral vibrations. By analyzing amplitude spectrum, it is clear that the system motion is quasi-periodic motion due to the appearance of combination frequency components about rotating frequency $1 \times$ (about 106 Hz) and a frequency component of 59 Hz denoted by f_{n1} . f_{n1} is related to the natural frequency of rotor and stator coupling system. The similar explanation about the mechanism of low subharmonic response in rotor-stator contact can also be found in Ref. [43]. Moreover, Ehrich [44] also pointed out that two base frequencies related to combination frequencies, one is usually synchronous with rotor speed (i.e., attributable to rotor unbalance) and the second might be associated with one of other vibration sources—unbalance of another shaft rotating at a different speed; rotor

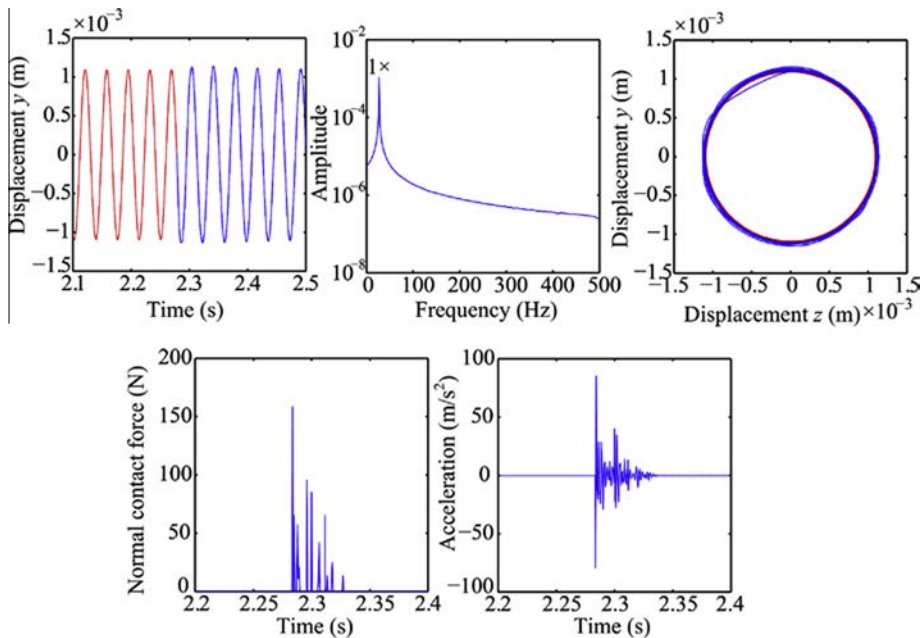


Fig. 10. Vibration responses of the rotor system with annular rubbing caused by sudden impact excitation under loading condition 1 (case 1).

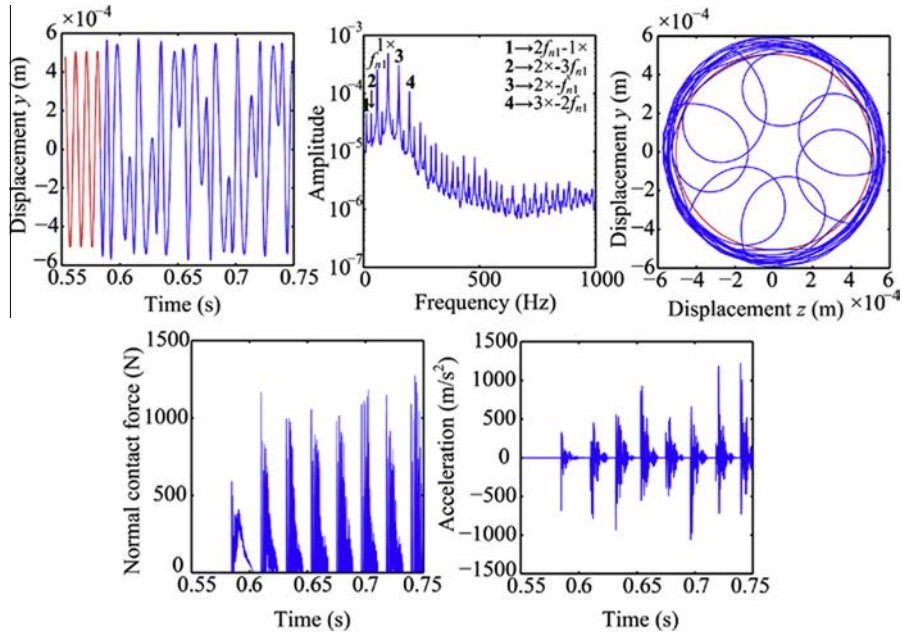


Fig. 11. Vibration responses of the rotor system with annular rubbing caused by sudden impact excitation under loading condition 2 (case 2).

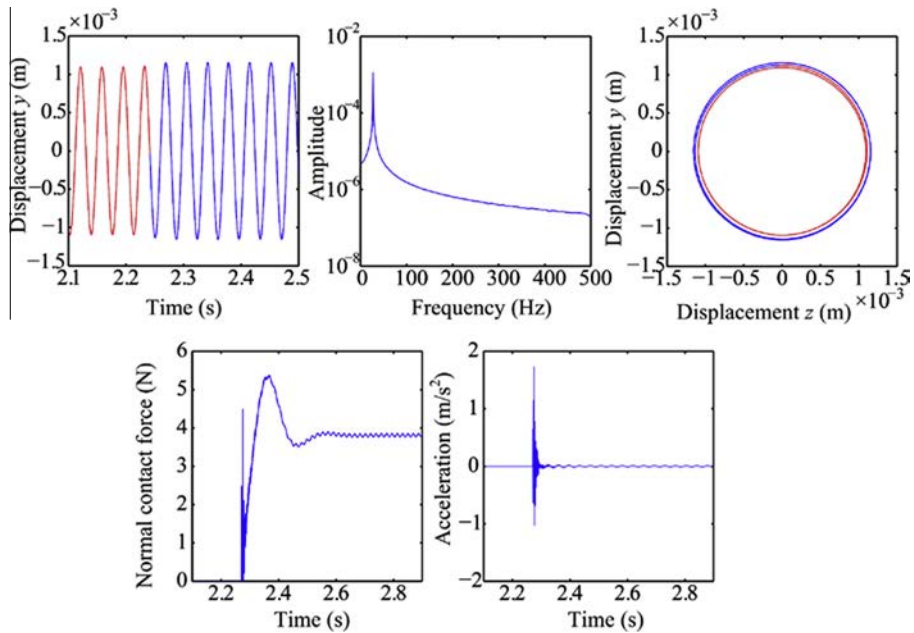


Fig. 12. Vibration responses of the rotor system with annular rubbing caused by sudden unbalance excitation under loading condition 1 (case 3).

whipping associated with trapped fluid in the rotor, or journal bearing instability, or hysteretic whirl, etc. The first lateral natural frequency of the rotor-stator system is about 69.9 Hz by jointing the stator and the rotor by a spring (simulation for the stator stiffness). Since the gap between the rotor and stator, the rotor-stator system stiffness is nonlinear and depends on the rotor and the stator orbits [43], the actual natural frequency will be lower than 69.9 Hz. Based on that, the authors think that the other vibration source of this system is the impact caused by rubbing, which excites the lateral free vibration of the rotor-stator system ($f_{n1} = 59$ Hz).

4.1.2. Sudden unbalance excitation

Rotor-stator gap ratio δ is the same as that under the sudden impact excitation. System vibration responses (case 3) caused by sudden unbalance excitation under loading condition 1 are shown in Fig. 12. The figure shows that the full annular

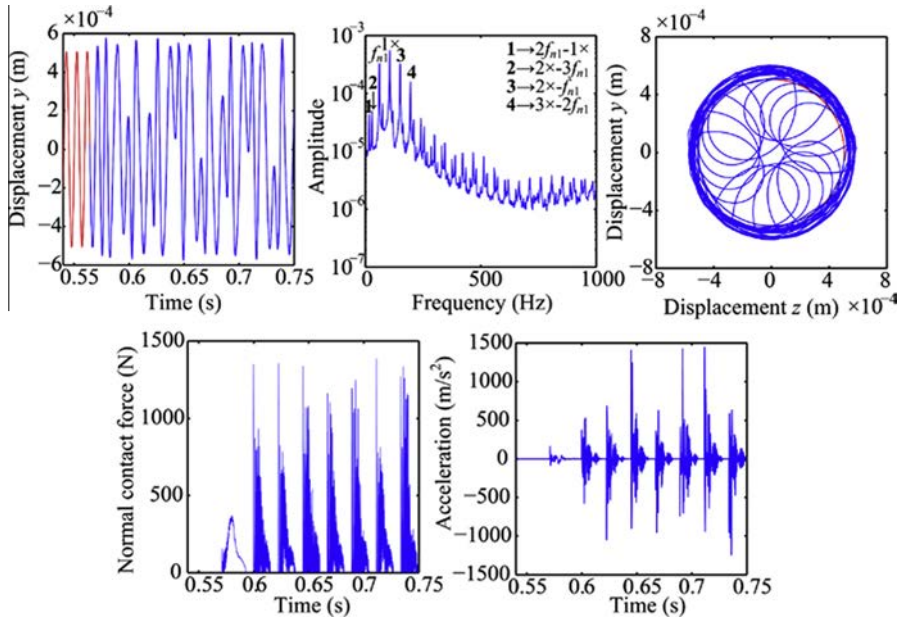


Fig. 13. Vibration responses of the rotor system with annular rubbing caused by sudden unbalance excitation under loading condition 2 (case 4).

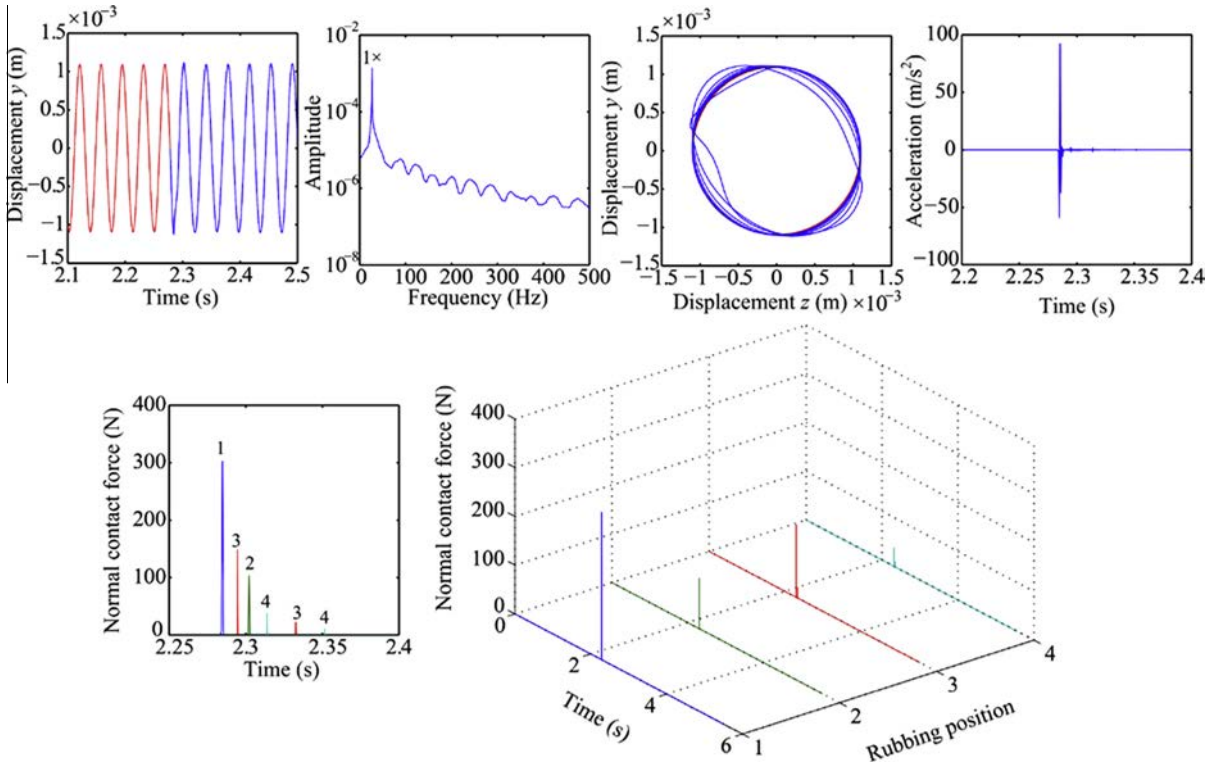


Fig. 14. Vibration responses of rotor system with four-point rubbing caused by sudden impact excitation under loading condition 1 (case 5).

rubbing appears when the rotor experiences transient impact. The normal rubbing force keeps stable at 3.8 N and the wave amplitude is about 0.5 N due to the continuous unbalance excitation. The similar simulation results about full annular rubbing can also be found in Ref. [22]. Vibration responses under case 4 are shown in Fig. 13, which is similar to those in Fig. 11. The collision degree is larger than that under case 2 by comparing the normal contact force and stator acceleration. The base

frequency of combination frequency f_{n1} changes from 59 Hz to 61 Hz. The main reason for the change is mainly due to the change of first lateral natural frequency of rotor stator system caused by rubbing.

4.2. Four point rubbing simulation

4.2.1. Sudden impact excitation

Assuming that δ for four pin shape stator (see Fig. 3(b)) is 1.01 under four point rubbing condition. System vibration responses with four point rubbing caused by the sudden impact excitation under loading condition 1 (case 5) are shown in Fig. 14. The above four figures from the left to the right, are the time domain waveform, amplitude spectrum, rotor orbit and the acceleration of the stator in the negative z direction, respectively. The below figures are the normal contact force under four rubbing directions where the numbers in abscissa of rubbing position denote the stator positions (see Fig. 3(b)). The layouts in Figs. 15–17 are the same as Fig. 14. The system vibration responses show that the first rubbing appears at z negative direction, the last rubbing at y positive direction, then disappears. The collision intensity gradually diminishes with the increasing collision times.

Vibration responses under case 6 are shown in Fig. 15. The figure shows that the system motion is complicated due to four unilateral constraints caused by rubbing. Rotor orbit is limited to a square and multiple loops are intertwined due to the rebound caused by impact. The first cluster of collision shows that the rotor contacts each stator two times and the collision intensity increases at first four times and decreases at later four times, which can be observed by normal contact force. Amplitude spectrum shows that the odd multiple frequency components, such as $3\times$ and $5\times$ and combination frequency components related to $1\times$ and f_{n1} ($f_{n1} = 64$ Hz) appear.

4.2.2. Sudden unbalance excitation

System vibration responses under case 7 are shown in Fig. 16. Compared with the vibration responses under case 3, it is clear that the rubbing forms are changed from full annular rubbing to partial fixed point rubbing. Rotor orbit indicates some slight bounces due to small normal contact forces. Frequency feature shows odd multiple frequencies, such as $3\times$, $5\times$ and $7\times$.

System vibration responses under case 8 are shown in Fig. 17. Compared with the vibration responses under case 4, it can be observed that the rotor rebound intensity is weakened and rotor orbit is similar to a square. Amplitude spectrum is similar to that under case 6, f_{n1} is 64 Hz and these combination frequency components are evenly distributed in both sides of $1\times$, $3\times$, $5\times$ and $7\times$. These odd multiple frequency components are dominant compared with these combinations frequency components. Moreover, the collision times under case 7 are also greater than those under case 6.

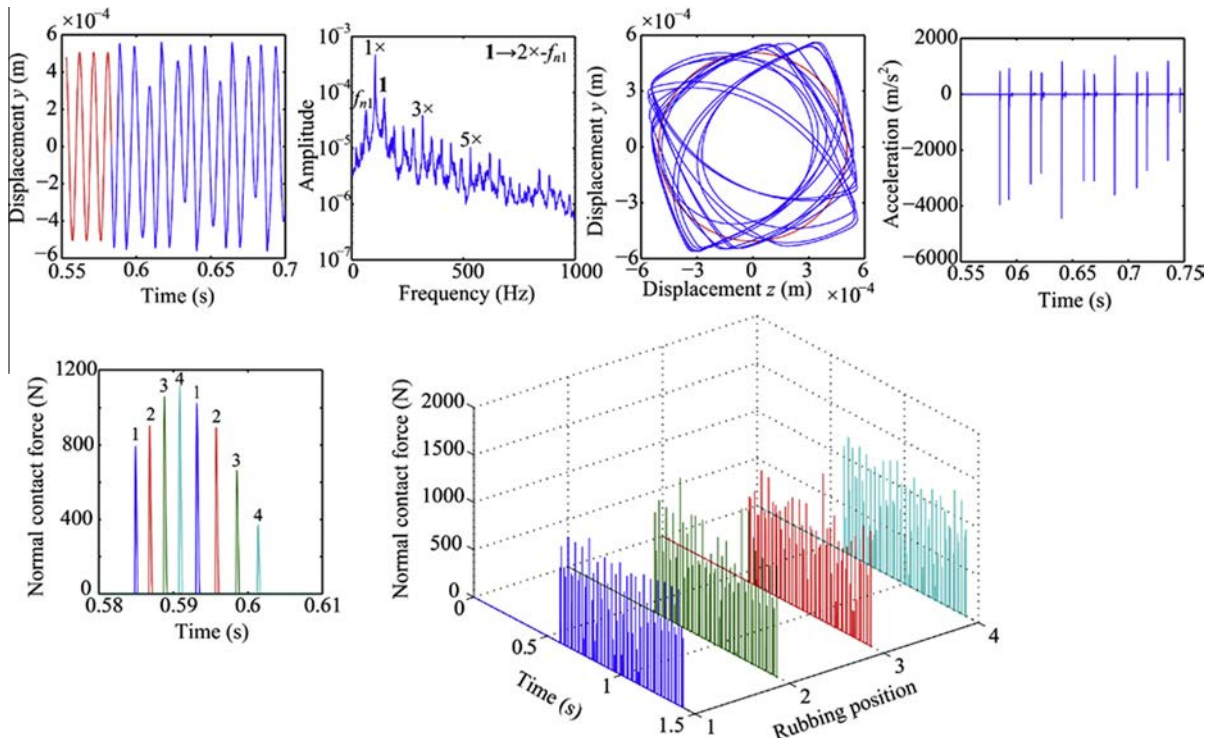


Fig. 15. Vibration responses of the rotor system with four-point rubbing caused by sudden impact excitation under loading condition 2 (case 6).

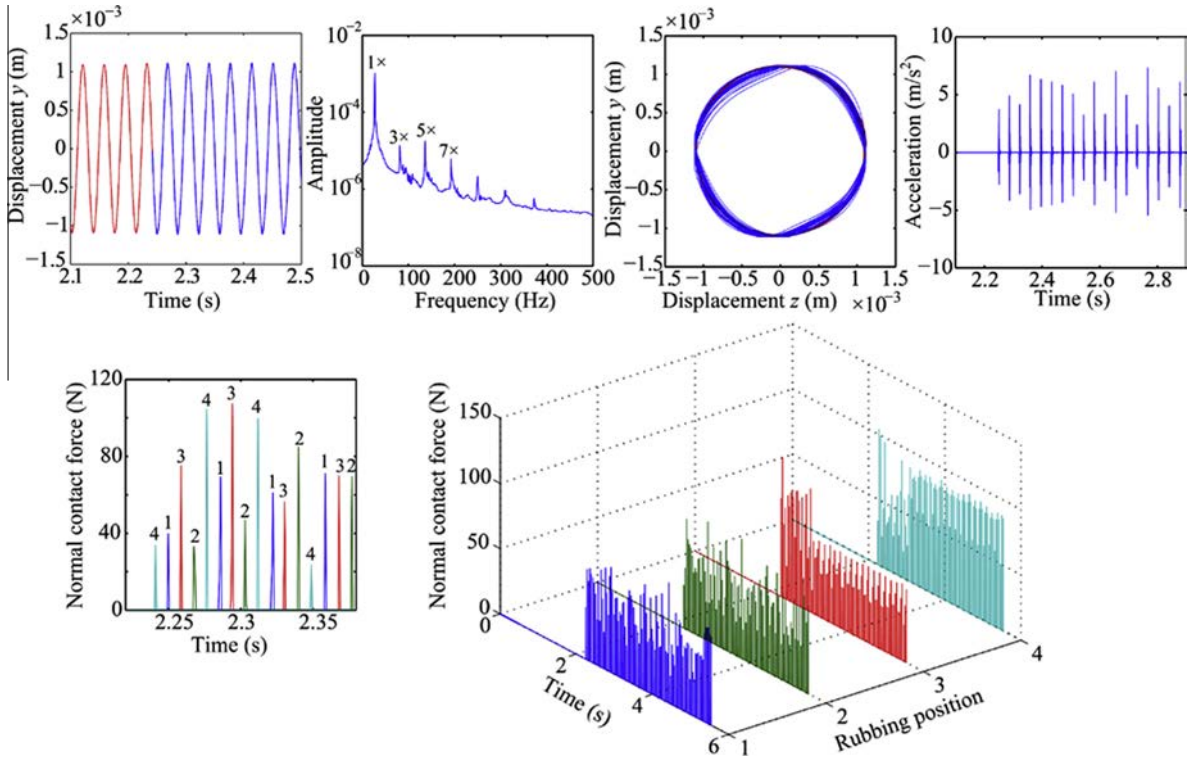


Fig. 16. Vibration responses of the rotor system with four-point rubbing caused by sudden unbalance excitation under loading condition 1 (case 7).

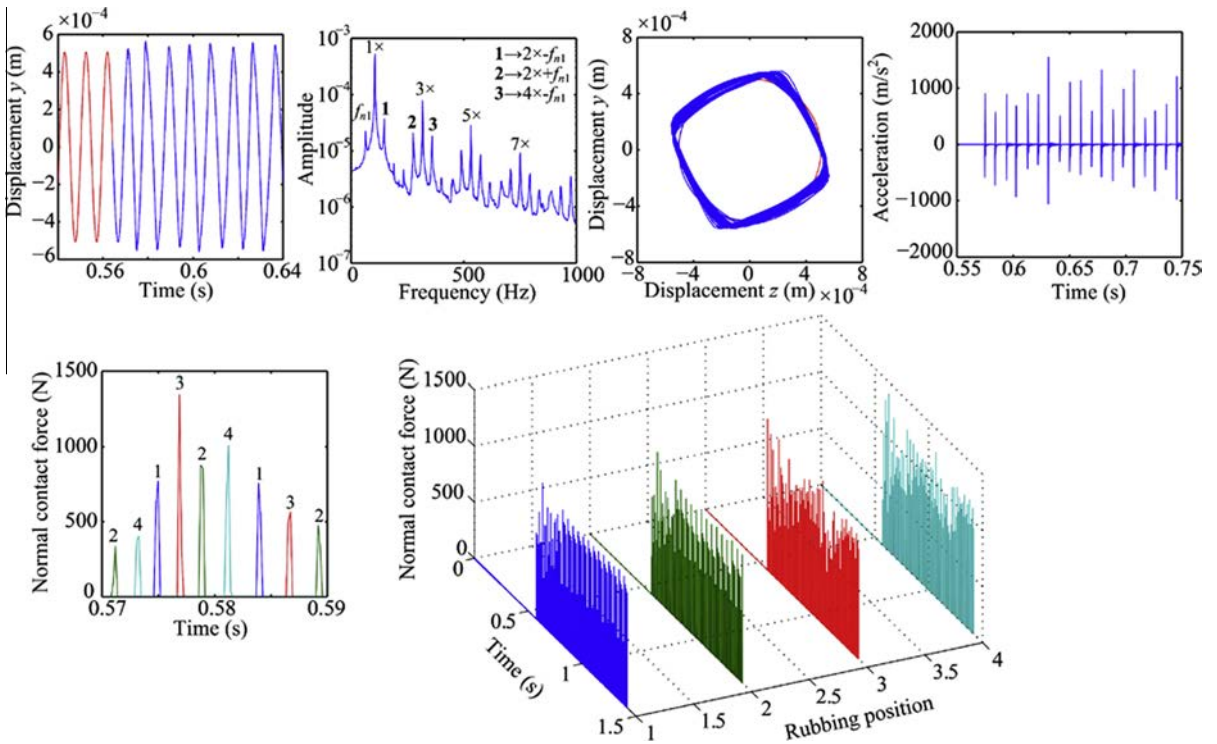


Fig. 17. Vibration responses of the rotor system with four-point rubbing caused by sudden unbalance excitation under loading condition 2 (case 8).

4.3. Results comparison

The above simulation results exhibit the following dynamic phenomena.

- (1) Comparing with simulation results under two loading conditions, it can be observed that the rubbing intensity under loading condition 1 is weaker than that under loading condition 2, which can be confirmed by the normal contact force and stator acceleration.
- (2) Comparing with rubbing simulation results caused by the sudden impact excitation and sudden unbalance excitation, it can be seen that the rubbing caused by the former will soon disappear under loading condition 1, however, it always exists under loading condition 2. Rubbing caused by the later will lead to full annular rubbing under loading condition 1 and partial unfixed point rubbing.
- (3) Comparing with the annular rubbing and four fixed point rubbing, it is clear that annular rubbing under loading condition 1 may cause full annular rubbing and will excite greater subsynchronous vibration; four fixed point rubbing under loading condition 1 will only excite odd multiple frequency components, such as $3\times$ and $5\times$, weaker subsynchronous vibration and greater odd multiple frequency components.

For the two types of rubbing, complicated combination frequency components related the rotating frequency $1\times$ and the first lateral natural frequency of the rotor stator coupling system f_{n1} can be observed under loading condition 2. Four fixed point rubbing will restrain the lower combination frequency components because it is easily to cause impact dominant rubbing, which is closely related to high multiple frequency components. f_{n1} gradually increases with the increasing rubbing intensity.

5. Conclusions

In this study, two finite element model of a rotor system with annular rubbing and four point rubbing are established. Assuming that rubbing is caused by the sudden impact excitation and sudden unbalance excitation, system dynamic characteristics are investigated based on contact dynamics theory under two loading conditions. Some conclusions drawn from the study can be summarized as follows:

- (1) The rubbing intensity under the first loading condition is weaker than that under the second loading condition. Rubbing caused by the sudden impact under loading condition 1 will soon disappear due to the action of damping dissipation energy. However, the rubbing caused by sudden impact under loading condition 2 will always exist because the partial rotational energy is translated to the rebound energy.
- (2) Rubbing under loading condition 2 will excite quasi periodic motion of the rotor system. Combination frequency components about the rotating frequency and the lateral natural frequency of rotor stator coupling system can be viewed as the most distinguishable characteristic.
- (3) Full annular rubbing may appear due to the sudden unbalance excitation under loading condition 1, such as case 3. Four point rubbing can avoid the hazard of full rubbing and restrain the subsynchronous vibration. Moreover, the acceleration of the stator can be used to evaluate the impact intensity, which is closely related to the normal contact force.

Numbers of the pin shape stators, such as three stators, and parameters studies, such as the rotor stator clearance, stator support stiffness, etc. are outside the scope of this study, and the focus is different dynamic characteristics caused by different rubbing forms. Moreover the effects related to shaft heating due to rubbing are also neglected. In future articles, emphasis will be given to the effects of real stator structural parameters and different contact models, considering thermal effects and friction torque during the rubbing.

Acknowledgments

This project is supported by Program for New Century Excellent Talents in University (Grant No. NCET 11 0078), the Fundamental Research Funds for the Central Universities (Grant No. N130403006) and the Joint Funds of the National Natural Science Foundation and the Civil Aviation Administration of China (Grant No. U1433109) for providing financial support for this work. The authors also thank the anonymous reviewers for their valuable comments.

Appendix A

A.1. Element matrixes of lumped mass used to simulate rotating disks

Mass matrix of the lumped mass element M_d^e is as follows:

$$\mathbf{M}_d^e = \text{diag}[m_d \ m_d \ I_d \ I_d], \quad (\text{A.1})$$

where m_d and I_d denote the mass and the diametral mass moment of inertia of the disk, respectively.

Gyroscopic matrix of the lumped mass element \mathbf{G}_d^e is as follows:

$$\mathbf{G}_d^e = \begin{bmatrix} 0 & 0 & 0 & 0 \\ 0 & 0 & 0 & 0 \\ 0 & 0 & 0 & I_p \\ 0 & 0 & I_p & 0 \end{bmatrix}, \quad (\text{A.2})$$

where I_p denotes the polar mass moment of inertia of the disk.

A.2. Element matrixes of the circular stator and the pin shape stators

The circular stator is simulated by a lumped mass element and its mass matrix \mathbf{M}_s^e is as follows:

$$\mathbf{M}_s^e = \text{diag}[m_s \ m_s], \quad (\text{A.3})$$

where m_s denote the mass in y and z directions, respectively.

Stiffness matrix \mathbf{K}_s^e is as follows:

$$\mathbf{K}_s^e = \text{diag}[k_{sy} \ k_{sz}], \quad (\text{A.4})$$

where k_{sy} and k_{sz} denote the stiffness coefficients in y and z directions, respectively.

The pin shape stators are simulated by beam element which only contains axial DOF and its mass matrix \mathbf{M}_s^e is as follows:

$$\mathbf{M}_s^e = \rho_s A_s l \begin{bmatrix} 1/3 & 1/6 \\ 1/6 & 1/3 \end{bmatrix}, \quad (\text{A.5})$$

ρ_s , A_s and l denote the stator density, cross section area and element length.

The stiffness matrix \mathbf{K}_s^e is as follows:

$$\mathbf{K}_s^e = \text{diag}\left[\frac{A_s E}{l} \ \frac{A_s E}{l}\right], \quad (\text{A.6})$$

E is the modulus of elasticity of stator.

Taking the pin shape stator in negative z direction for example, the support stiffness matrix of the stator \mathbf{K}_{ss}^e is as follows:

$$\mathbf{K}_{ss}^e = \text{diag}[k_{sz} \ k_{sz}], \quad (\text{A.7})$$

where k_{sz} denotes the axial stiffness coefficient of the stator in z direction.

The support damping matrix of the stator \mathbf{C}_{ss}^e is as follows:

$$\mathbf{C}_{ss}^e = \text{diag}[c_{sz} \ c_{sz}], \quad (\text{A.8})$$

where c_{sz} denotes the axial damping coefficient of the stator in z direction. Similarly, other pin shape stators have the same element forms as the sample.

References

- [1] H. Han, Z. Zhang, B. Wen, Periodic motions of a dual-disc rotor system with rub-impact at fixed limiter, Proc. Inst. Mech. Eng., Part C: J. Mech. Eng. Sci. 222 (2008) 1935–1946.
- [2] H. Ma, C. Shi, Q. Han, et al, Fixed-point rubbing fault characteristic analysis of a rotor system based on contact theory, Mech. Syst. Signal Process. 38 (2013) 137–153.
- [3] S. Lahriri, H. Weber, I. Santos, et al, Rotor-stator contact dynamics using a non-ideal drive-theoretical and experimental aspects, J. Sound Vib. 331 (2012) 4518–4536.
- [4] S. Lahriri, I. Santos, H. Weber, et al, On the nonlinear dynamics of two types of backup bearings-theoretical and experimental aspects, J. Eng. Gas Turbines Power 134 (2012) 112503.1–112503.13.
- [5] M. Behzada, M. Alvandi, D. Mba, et al, A finite element-based algorithm for rubbing induced vibration prediction in rotors, J. Sound Vib. 332 (2013) 5523–5542.
- [6] J. Isaksson, A. Frid, Analysis of dynamical behaviour of a rotor with deflection limiters, Acta Mech. 133 (1999) 1–11.
- [7] J. Zapomel, C. Fox, E. Malenovsky, Numerical investigation of a rotor system with disc-housing impact, J. Sound Vib. 243 (2001) 215–240.
- [8] R. Beatty, Differentiating rotor response due to radial rubbing, J. Vib. Acoust. Stress Reliab. Des. 107 (1985) 151–160.
- [9] M. Torkhani, L. May, P. Voinis, Light, medium and heavy partial rubs during speed transients of rotating machines: numerical simulation and experimental observation, Mech. Syst. Signal Process. 29 (2012) 45–66.
- [10] M. Abuzaid, M. Eleshaky, M. Zedan, Effect of partial rotor-to-stator rub on shaft vibration, J. Mech. Sci. Technol. 23 (2009) 170–182.
- [11] Y. Choi, On the contact of partial rotor rub with experimental observations, J. Mech. Sci. Technol. 15 (2001) 1630–1638.
- [12] P. Pennacchi, N. Bachschmid, E. Tanzi, Light and short arc rubs in rotating machines: experimental tests and modelling, Mech. Syst. Signal Process. 23 (2009) 2205–2227.
- [13] W. Zhang, G. Meng, et al, Nonlinear dynamics of a rub-impact micro-rotor system with scale-dependent friction model, J. Sound Vib. 309 (2008) 756–777.
- [14] S. Popprath, H. Ecker, Nonlinear dynamics of a rotor contacting an elastically suspended stator, J. Sound Vib. 308 (2007) 767–784.

- [15] T. Patel, M. Zuo, X. Zhao, Nonlinear lateral-torsional coupled motion of a rotor contacting a viscoelastically suspended stator, *Nonlinear Dyn.* 69 (2012) 325–339.
- [16] F. Chu, W. Lu, Experimental observation of nonlinear vibrations in a rub-impact rotor system, *J. Sound Vib.* 283 (2005) 621–643.
- [17] N. Bachschmid, E. Tanzi, M. Santos et al., Some experimental results in rubbing phenomena analysis, in: *Proceedings of the XII International Symposium on Dynamic Problems of Mechanics (DINAME 2007)*, 2007.
- [18] Y. Choi, Investigation on the whirling motion of full annular rotor rub, *J. Sound Vib.* 258 (2002) 191–198.
- [19] J. Jiang, H. Ulbrich, Stability analysis of sliding whirl in a nonlinear Jeffcott rotor with cross-coupling stiffness coefficients, *Nonlinear Dyn.* 24 (2001) 269–283.
- [20] D. Childs, D. Kumar, Dry-friction whip and whirl predictions for a rotor-stator model with rubbing contact at two locations, *J. Eng. Gas Turbines Power* 134 (2012) 072502.1–072502.11.
- [21] J. Yu, On occurrence of reverse full annular rub, *J. Eng. Gas Turbines Power* 134 (2012) 012505.1–012505.8.
- [22] O. Grapis, V. Tamuzs, N. Ohlson, et al, Overcritical high-speed rotor systems, full annular rub and accident, *J. Sound Vib.* 290 (2006) 910–927.
- [23] W. Lu, F. Chu, Radial and torsional vibration characteristics of a rub rotor, *Nonlinear Dyn.* 76 (2014) 529–549.
- [24] X. Dai, X. Zhang, X. Jin, The partial and full rubbing of a flywheel rotor-bearing-stop system, *Int. J. Mech. Sci.* 43 (2001) 505–519.
- [25] W. Kellenberger, Spiral vibrations due to the seal rings in turbogenerators thermally induced interaction between rotor and stator, *J. Mech. Des.* 102 (1980) 177–184.
- [26] D. Childs, Clearance effects on spiral vibrations due to rubbing, in: *Proceedings of the 1997 ASME Design Engineering Conferences, DETC-97, 16th Biennial Conference on Mechanical Vibration and Noise, Sacramento, CA, 1997*, pp. 1–9.
- [27] P. Goldman, A. Muszynska, Rotor to stator, rub-related, thermally/mechanical effects in rotating machinery, *Chaos Solitons Fract.* 5 (1995) 1579–1601.
- [28] J. Sawicki, A. Montilla-Bravo, Z. Gosiewski, Thermomechanical behavior of rotor with rubbing, *Int. J. Rotating Mach.* 9 (2003) 41–47.
- [29] Y. Tian, J. Yang, Research on vibration induced by the coupled heat and force due to rotor-to-stator rub, *J. Vib. Control* 17 (2010) 549–566.
- [30] N. Bachschmid, P. Pennacchi, A. Vania, Thermally induced vibrations due to rub in real rotors, *J. Sound Vib.* 299 (2007) 683–719.
- [31] S. Chen, M. Geradin, Finite element simulation of non-linear transient response due to rotor-stator contact, *Eng. Comput.* 14 (6) (1997) 591–603.
- [32] A. Chavez, H. Ulbrich, L. Ginzinger, Reduction of contact forces in a rotor-stator-system in case of rubbing through active auxiliary bearing, *Shock Vib.* (2006) 505–518.
- [33] L. Ginzinger, H. Ulbrich, Control of rubbing rotor using an active auxiliary bearing, *J. Mech. Sci. Technol.* 21 (2007) 851–854.
- [34] M. Sahinkaya, A. Abulrub, P. Keogh, et al, Multiple sliding and rolling contact dynamics for a flexible rotor/magnetic bearing system, *IEEE/ASME Trans. Mechatron.* 12 (2007) 179–189.
- [35] S. Roques, M. Legrand, et al, Modeling of a rotor speed transient response with radial rubbing, *J. Sound Vib.* 329 (2010) 527–546.
- [36] D. Xu , *A new node-to-node approach to contact/impact problems for two dimensional elastic solids subject to finite deformation (Ph.D. thesis)*, The University of Illinois at Urbana-Champaign, 2008.
- [37] J. Simo, T. Laursen, An augmented Lagrangian treatment of contact problems involving friction, *Comput. Struct.* 42 (1) (1992) 97–116.
- [38] T. Laursen, *Computational Contact and Impact Mechanics: Fundamentals of Modeling Interfacial Phenomena in Nonlinear Finite Element Analysis*, Springer, Berlin, 2003.
- [39] K. Bathe, E. Wilson, *Numerical Methods in Finite Element Analysis*, Prentice-Hall Inc., New Jersey, 1976.
- [40] H. Ma, J. Yang, R.Z. Song, et al, Effects of tip relief on vibration responses of a geared rotor system, *Proc. Inst. Mech. Eng., Part C: J. Mech. Eng. Sci.* 228 (2014) 1132–1154.
- [41] A. Muszynska, *Rotordynamics*, CRC Taylor & Francis Group, New York, 2005, p. 657–661.
- [42] *API 617, Axial and centrifugal compressors and turboexpanders for petroleum, chemical and gas industry services*, American Petroleum Institute, Washington DC, 2002.
- [43] G. Groll, D. Ewins, A mechanism of low subharmonic responses in rotor/stator contact – measurements and simulations, *J. Vib. Acoust.* 124 (2002) 350–358.
- [44] F. Ehrlich, Sum and difference frequencies in vibration of high speed rotating machinery, *J. Eng. Ind.* 94 (1972) 181–184.